

# Close binary evolution

## I. The tidally induced shear mixing in rotating binaries

H.F. Song,<sup>1,2,4</sup> A. Maeder<sup>2</sup>, G. Meynet<sup>2</sup>, R.Q. Huang<sup>3</sup>, S. Ekström<sup>2</sup> and A. Granada<sup>2</sup>

<sup>1</sup> College of Science, Guizhou University, Guiyang, Guizhou Province, 550025, P.R. China  
e-mail: songhanfeng@163.com; sci.hfsong@gzu.edu.cn

<sup>2</sup> Geneva Observatory, Geneva University, CH-1290 Sauverny, Switzerland

<sup>3</sup> National Astronomical Observatories/Yunnan Observatory, the Chinese Academy of Sciences, Kunming, Yunnan Province, 650011, P.R. China

<sup>4</sup> Key Laboratory for the Structure and Evolution of Celestial Objects, Chinese Academy of Sciences, Kunming, 650011, P.R. China

Received; accepted

### ABSTRACT

*Context.* Tides are known to play a great role in binary evolution, leading in particular to synchronisation of axial and orbital rotations and to binary mass transfer.

*Aims.* We study how tides in a binary system induce some specific internal shear mixing, able to substantially modify the evolution of close binaries prior to mass transfer.

*Methods.* We construct numerical models accounting for tidal interactions, meridional circulation, transport of angular momentum, shears and horizontal turbulence and consider a variety of orbital periods and initial rotation velocities.

*Results.* Depending on orbital periods and rotation velocities, tidal effects may spin down (spin down Case) or spin up (spin up Case) the axial rotation. In both cases, tides may induce a large internal differential rotation. The resulting tidally induced shear mixing (TISM) is so efficient that the internal distributions of angular velocity and chemical elements are greatly influenced. The evolutionary tracks are modified, and in both cases of spin down and spin up, large amounts of nitrogen can be transported to the stellar surfaces before any binary mass transfer. Meridional circulation, when properly treated as an advection, always tends to counteract the tidal interaction, tending to spin up the surface when it is braked down and vice versa. As a consequence, **the times needed for the axial angular velocity to become equal to the orbital angular velocity may be larger than given by typical synchronization timescales. Also, due to meridional circulation some differential rotation remains in tidally locked binary systems.**

**Key words.** binaries:close-stars; stars: abundances; rotation;evolution

## 1. Introduction

Rotation is an important factor to be considered in the evolution of massive stars (Kippenhahn & Thomas 1970; Endal & Sofia 1976; Meynet & Maeder 1997; Langer 1998). The centrifugal force not only gives the star an oblate shape, but it also induces many instabilities leading to the

mixing of chemical elements in the stellar interiors (Maeder & Meynet 2000; Heger, Langer & Woosley 2000a; Huang 2004a,b). In addition to convection and semi-convection, there are several processes which may contribute to the mixing of the chemical elements in stellar interiors, such as shears due to internal differential rotation, meridional circulation, magnetic instabilities, magnetic braking at the surface of the star which favors large shears (Chaboyer & Zahn 1992; Zahn 1992; Maeder & Meynet 2001,2005; Meynet et al. 2011; Mathis et al. 2004a,b). These physical processes are active both in single and binary stars. They may have important consequences on observable properties (Langer & Maeder 1995; Heger & Langer 2000b; Song et al. 2009, 2011). They can mix the material of the core and envelope leading, among other consequences, to nitrogen enrichment at the stellar surface. Many B- and O-type stars show nitrogen excesses (Walborn 1976; Heap et al. 2006; Hunter et al. 2009; Przybilla et al. 2010) and the mentioned instabilities may play a role in these facts.

Recent results suggest that the half of the massive stars in the Tarentula region may exchange mass with a binary companion, thus potentially largely affecting the course of stellar evolution through tides, mass transfer and mergers (Sana et al. 2013; de Mink et al. 2013). The fraction of binary systems, and the fraction of short period O-type stars, are largely varying in different clusters (Mahy et al. 2009), the binary properties being possibly related to the density of the clusters.

Many physical effects studied in the context of single star evolution need also to be considered in the framework of binary evolution. Here we concentrate on the interaction of some effects of rotation, such as meridional circulation, shears, and horizontal turbulence, with binary evolution. In particular, the tidally induced shear mixing (hereafter called TISM) may be important in binary evolution. The tidal interactions produce braking, particularly in the outer stellar layers and thus may enhance the internal differential rotation. The instabilities associated to large shears result in a significant transport of the chemical elements. In the present work we want to investigate how the tidal braking and its related effects, in particular TISM, can affect the evolution of close binaries.

On top of that, meridional circulation, when correctly treated as a circulation and not as a diffusion, often reacts in an interesting way, by even being able to transport angular momentum from regions with low rotation to regions where rotation is fast (Maeder 2009). Thus, by studying TISM in the framework of models where meridional circulation is consistently treated, we may see the reactions of the star to the interaction of meridional circulation and tidal braking. These effects, which were not foreseen, appear to play a significant role in binary evolution.

The paper is organized as follows: The tidal braking is presented in Section 2. The equations expressing internal transport of chemical elements and angular momentum are presented in Section 3. In Section 4, the results of numerical calculation are described and discussed in details. Finally in Section 5, conclusions are made.

## 2. Tidal interactions in rotating binaries

One may distinguish the equilibrium and dynamical tides (Zahn 1966; Zahn 1975). For not yet synchronised systems, subject to the effects of dynamical tides, the dissipation mechanisms play a major role. These are typically the viscous effect of turbulence in stars with a convective envelope and the radiative damping for stars with a radiative envelope (Zahn 1977). A new expression for

the tidal synchronisation timescale due to a turbulent medium has been proposed by Toledano et al. (2007),

$$\tau_{\text{sync,turb}} = f_{\text{turb}} q^{-2} \left(\frac{R}{a}\right)^{-6} \text{year}, \quad (1)$$

where  $a$  is the separation between the two components in a binary system,  $f_{\text{turb}} \sim 1$  depends on the structure of the star. Equation (1) can be applied to stars with an envelope hosting a strong turbulence due to convection and, maybe, due to rotational instabilities, such as the horizontal turbulence proposed by Zahn (1992). However, the adequation of this expression to this last case is still under question, since the viscous effect of horizontal turbulence is about 8 orders of magnitude smaller than the viscosity of classical convection in massive stars.

The dynamical synchronisation timescale due to radiative damping for stars with a radiative envelope, **without the contribution of the equilibrium tide**, has been given by (Zahn 1977),

$$\tau_{\text{sync,rad}} = \frac{1}{5 \times 2^{5/3} q^2 (1+q)^{5/6} E_2} \left(\frac{R^3}{GM}\right)^{1/2} \beta \left(\frac{a}{R}\right)^{17/2}. \quad (2)$$

Here,  $q = M'/M$  is the mass ratio,  $M'$  is the mass of the companion star,  $R$  and  $M$  are the radius and mass of the primary star considered here,  $G$  is the gravity constant,  $\beta = I_e/MR^2$  is the so-called gyration radius,  $I_e$  is the moment of inertia of the external layers where tidal energy is dissipated, and  $E_2$  is the tidal coefficient, which is sensitive to the structure of the star, in particular to the size of the convective core. It can be expressed by (Yoon, Woosley & Langer 2010)

$$E_2 \sim 10^{-1.37} \left(\frac{R_{\text{conv}}}{R}\right)^8, \quad (3)$$

where  $R_{\text{conv}}$  is the convective-core radius.

A comparison of the above two dissipation timescales (Eqs 1 and 2), for the turbulent and radiative cases, has been performed by de Mink et al. (2009).

**In the present work, the change of the spin angular momentum due to tidal interaction is computed using Eq. (5.6) from Zahn (1977):**

$$\frac{dI_e \Omega}{dt} = -3MR^2 (\Omega - \omega_{\text{orb}}) \left(\frac{GM}{R^3}\right)^{1/2} \left[q^2 \left(\frac{R}{a}\right)^6\right] E_2 S_{22}^{5/3}, \quad (4)$$

where  $I_e \Omega$  is the angular momentum of the external layers where tidal energy is dissipated,  $\Omega$  and  $\omega_{\text{orb}}$  are respectively the angular velocity of axial and orbital rotation. Tidal interactions spin the star down when  $\Omega > \omega_{\text{orb}}$  and up when  $\Omega < \omega_{\text{orb}}$ .

Rigorously speaking, the effect of tidal braking should be applied to the whole radiative envelope. As some differential rotation is generally present, there may be some deviations from the above current expressions for tidal braking. However, some approximations are justified. In our current models, we treat a limited fraction of the outer layers (about 3% of the total mass) with the assumptions of constant chemical abundances  $X_i = \text{const.}$ , constant luminosity  $L = \text{const.}$ , and angular velocity  $\Omega = \text{const.}$  These homogeneous outer layers of small mass content may encompass about 30% of the total radius, which implies that about 92% of the total tidal effect (going like  $R^6$ ) is deposited in these layers (for a value of 20% of the radius, the deposited fraction would be 79%). This means that most of the energy dissipated by the tidal torque is deposited in the outer layers, where the angular velocity is anyway taken as a constant. So the various approximations made in the models are internally consistent.

Assuming  $I_e$  and  $\omega_{\text{orb}}$  are constant in Eq. (4), we can obtain,  $t_{\text{rot}}$ , the typical timescale for a decrease by a factor  $e$  of the difference between  $\Omega$  and  $\omega$ ,

$$-\frac{1}{(\Omega - \omega_{\text{orb}})} \frac{d(\Omega - \omega_{\text{orb}})}{dt} = \frac{1}{t_{\text{rot}}}, \quad (5)$$

with

$$\frac{1}{t_{\text{rot}}} = 3 \left( \frac{GM}{R^3} \right)^{1/2} \frac{MR^2}{I_e} E_2 \left[ q^2 \left( \frac{R}{a} \right)^6 \right] s_{22}^{5/3}. \quad (6)$$

The synchronization rate  $t_{\text{rot}}^{-1}$  is a function of both the strength of the perturbing potential as measured by the quantity in brackets  $[q^2 (\frac{R}{a})^6]$ , and of the tidal frequency  $s_{22} = 2(\Omega - \omega_{\text{orb}}) (\frac{R^3}{GM})^{1/2}$ .

In the rest of the paper, we shall call  $t_{\text{rot}}$ , the synchronization timescale (implicitly estimated on the ZAMS), while the time, given by the present evolutionary models, at which  $\Omega = \omega_{\text{orb}}$  will be named the effective synchronization time. The two times may be quite different since they do not encompass the same physics:  $t_{\text{rot}}$  only accounts for the change of  $\Omega$  due to the tidal interaction and is estimated for initial values on the ZAMS, while the synchronization time accounts for the changes with time of  $\Omega - \omega_{\text{orb}}$  and for the evolutions with time of all the quantities involved in the expressions of  $t_{\text{rot}}$ , as well as for all the other processes (in addition to tidal interactions) modifying the surface angular velocity of the star (changes of the radius of the star and all the processes redistributing the angular momentum inside the star).

In the case of a circular orbit, the orbital angular momentum of a binary with a orbital separation  $a$  is given by

$$J_{\text{orb}} = M_1 M_2 \left[ \frac{Ga}{M_1 + M_2} \right]^{1/2}, \quad (7)$$

so that

$$\frac{\dot{a}}{a} = \frac{2\dot{J}_{\text{orb}}}{J_{\text{orb}}} - 2\frac{\dot{M}_1}{M_1} - 2\frac{\dot{M}_2}{M_2} + \frac{\dot{M}_1 + \dot{M}_2}{M_1 + M_2}, \quad (8)$$

where a dot indicates time derivation.

### 3. Internal transport of chemical elements and of angular momentum

#### 3.1. The equation for angular momentum transport

The transport of angular momentum inside a star is implemented following the prescription of Zahn (1992). This prescription was complemented by Talon & Zahn (1997) and Maeder & Zahn (1998). In the radial direction, it obeys the equation

$$\rho \frac{d}{dt} (r^2 \bar{\Omega})_{M_r} = \frac{1}{5r^2} \frac{\partial}{\partial r} (\rho r^4 \bar{\Omega} U(r)) + \frac{1}{r^2} \frac{\partial}{\partial r} (\rho D r^4 \frac{\partial \bar{\Omega}}{\partial r}). \quad (9)$$

The first term on the right hand side of this equation is the divergence of the advected flux of angular momentum, while the second term is the divergence of the diffused flux.  $D$  is the total diffusion coefficient in the vertical direction, taking into account the various instabilities that transport angular momentum. The effects of expansion or contraction are automatically included in a Lagrangian treatment. During the evolution, central density increases and the core spin faster, the second term allows, for example, the transport of angular momentum from the core to the surface. It will also

transmit the external braking to the interior of the star. The meridional circulation is most efficient for such transports, its velocity was determined by Zahn (1992) and Maeder & Zahn (1998),

$$U(r) = \frac{P}{\rho g C_P T} \frac{1}{[\nabla_{\text{ad}} - \nabla_{\text{rad}} + (\varphi/\delta)\nabla_{\mu}]} \left[ \frac{L(r)}{M_{\star}(r)} (E_{\Omega}^{\star} + E_{\mu}) + \frac{C_P}{\delta} \frac{\partial \Theta}{\partial r} \right], \quad (10)$$

where  $C_P$  is the specific heat at constant pressure,  $\nabla_{\text{ad}} = \frac{P\delta}{\rho T C_P}$  is the adiabatic gradient,  $M_{\star} = M(1 - \frac{\Omega^2}{2\pi g \rho_m})$ , and  $\Theta = \tilde{\rho}/\bar{\rho}$  is the ratio of the variation of the density to the average density on an equipotential. Both  $\varphi$  and  $\delta$  arise from the equation of state in the form  $\frac{d\rho}{\rho} = \alpha \frac{dP}{P} + \varphi \frac{d\mu}{\mu} - \delta \frac{dT}{T}$ , and  $E_{\Omega}$  and  $E_{\mu}$  are terms that depend on the  $\Omega$ - and  $\mu$ -distributions respectively. The quantities  $E_{\Omega}^{\star}$  and  $E_{\mu}$  are given by (Maeder 2009)

$$\begin{aligned} E_{\Omega}^{\star} = & 2 \left[ 1 - \frac{\bar{\Omega}^2}{2\pi G \bar{\rho}} - \frac{\bar{\epsilon} + \bar{\epsilon}_{\text{grav}}}{\epsilon_m} \right] \frac{\bar{\rho}}{g} - \frac{\rho_m}{\bar{\rho}} \left\{ \frac{r}{3} \frac{d}{dr} [H_T \frac{d}{dr} (\frac{\Theta}{\delta})] \right. \\ & - \chi_T \Theta + (1 - \frac{1}{\delta}) \Theta \left. \right\} - \frac{2H_T}{r} (\frac{\Theta}{\delta}) + \frac{2}{3} \Theta \left. \right\} \\ & - \frac{\bar{\epsilon} + \bar{\epsilon}_{\text{grav}}}{\epsilon_m} [H_T \frac{d}{dr} (\frac{\Theta}{\delta}) + (f_{\epsilon} \epsilon_T - \chi_T) (\frac{\Theta}{\delta})] \\ & + (2 - f_{\epsilon} - \frac{1}{\delta}) \Theta, \end{aligned} \quad (11)$$

with

$$\begin{aligned} E_{\mu} = & \frac{\rho_m}{\bar{\rho}} \left\{ \frac{r}{3} \frac{d}{dr} [H_T \frac{d}{dr} (\frac{\varphi}{\delta} \Lambda)] - (\chi_{\mu} + \frac{\varphi}{\delta} \chi_T + \frac{\varphi}{\delta}) \Lambda \right. \\ & \left. - \frac{2H_T}{r} \frac{\varphi}{\delta} \Lambda \right\} + \frac{\bar{\epsilon} + \bar{\epsilon}_{\text{grav}}}{\epsilon_m} [H_T \frac{d}{dr} (\frac{\varphi}{\delta} \Lambda)] \\ & + (f_{\epsilon} \epsilon_{\mu} + f_{\epsilon} \frac{\varphi}{\delta} \epsilon_T - \chi_{\mu} - \frac{\varphi}{\delta} \chi_T - \frac{\varphi}{\delta}) \Lambda, \end{aligned} \quad (12)$$

where the quantities have the same significations as in Maeder & Zahn (1998). **We have taken the same boundary conditions as Talon et al. (1997; see also Denissenkov et al. 1999; Meynet & Maeder 2000).**

### 3.2. The equation for the transport of chemical species

The horizontal turbulence competes efficiently with the advective term of meridional circulation for transporting the chemical species (Chaboyer & Zahn 1992). The horizontal flow tends to homogenize the layers in such a way that the resulting transport of chemical species by both meridional circulation and horizontal turbulence can be computed as a diffusive process with the coefficient  $D_{\text{eff}}$ . The change of the abundance for a given chemical element  $i$  in the shell with coordinate  $r$  is thus (Zahn 1992):

$$\rho \frac{dX_i}{dt} = \frac{1}{r^2} \frac{\partial}{\partial r} [\rho r^2 (D + D_{\text{eff}}) \frac{\partial X_i}{\partial r}] + (\frac{dX_i}{dt})_{\text{nucl}}, \quad (13)$$

where  $D$  is the same as in Eq.(8) and is the total diffusion coefficient in the vertical direction, taking into account the instabilities that transport the chemical elements. The last term accounts for the change in abundances produced by nuclear reactions. We can then define an effective diffusion coefficient,  $D_{\text{eff}}$  that combines the effects of horizontal diffusion and of the meridional circulation (Chaboyer & Zahn 1992),

$$D_{\text{eff}} = \frac{1}{30} \frac{|r U(r)|^2}{D_h}. \quad (14)$$

We have applied the shellular-rotation hypothesis, which postulates that in differentially rotating stars the angular velocity  $\Omega$  is constant on isobars. This results from the strong horizontal turbulence, which is expected because there is no restoring force in the horizontal (isobaric) direction, as

the buoyancy force (the restoring force of the density gradient) acts in the vertical direction. Zahn (1992) relates the diffusion coefficient to the viscosity caused by horizontal turbulence

$$D_h \approx \nu_h = \frac{1}{c_h} r |2V(r) - \alpha U(r)|, \quad (15)$$

where  $c_h$  is a constant of the order of 1,  $V(r)$  is the horizontal component of the meridional circulation velocity,  $U(r)$  its vertical component (see Eq.9), and in this expression  $\alpha = \frac{1}{2} \frac{d \ln(r^2 \Omega)}{d \ln r}$ .

Differential rotation induces shear turbulence at the interface of layers that have different rotational velocities. A layer remains stable if the excess of kinetic energy due to differential rotation is inferior to the energy needed to overcome the stabilizing density gradient in radiative zones (this is expressed by the *Richardson criterion*). The effects of thermal dissipation, which reduce the buoyancy force, are accounted for. The coefficient of diffusion by shear turbulence was determined by Maeder (1997)

$$D_{\text{shear}} = f_{\text{energy}} \frac{H_p}{g \delta} \frac{K}{[\frac{\varphi}{\delta} \nabla_\mu + (\nabla_{\text{ad}} - \nabla_{\text{rad}})]} \left( \frac{9\pi}{32} \Omega \frac{d \ln \Omega}{d \ln r} \right)^2, \quad (16)$$

where  $K = \frac{4acT^3}{3kp^2C_p}$  is the thermal diffusivity, and with  $f_{\text{energy}} \approx 1$ , and  $\varphi = \left( \frac{d \ln \rho}{d \ln \mu} \right)_{P,T}$ .

#### 4. Physical ingredients of the models

The treatment of rotation was developed in a series of papers published previously by the Geneva group (Maeder 1999, 1997; Maeder & Meynet 2000; Maeder & Zahn 1998; Meynet & Maeder 1997, 2000; see also the recent review by Maeder & Meynet 2012).

The initial abundances of H, He, and metals are set to  $X=0.720$ ,  $Y=0.266$ , and  $Z=0.014$ . The mixture of heavy elements is that by Asplund et al. (2005) except for the Ne abundance, which is taken from Cunha et al. (2006). The nuclear reaction rates are generated with the NetGen tool<sup>1</sup>. They originate mainly from the Nacre database (Angulo et al. 1999), although some have been redetermined more recently and updated (see Ekström et al. 2012 for more details). The convective zones are determined with the Schwarzschild criterion. For the H- and He-burning phases, the convective core is extended by overshooting over a distance  $d_{\text{over}} = 0.10H_p$ , with  $H_p$  the local pressure scale height.

The evolution of a binary system consisting of a 15 and a 10  $M_\odot$  star is investigated in this paper. We assume that the orbit is circular and that the spin axis of the model stars is perpendicular to the orbital plane. We focus on the evolution of the primary star. From Eq. (7), assuming that the mass loss by stellar winds is negligible before any mass transfer, one has for the cases considered here that

$$\frac{\dot{a}}{a} = \frac{2J_{\text{orb}}}{J_{\text{orb}}} \simeq \frac{10^{-2} - 10^{-3}}{10^7 \text{ years}}, \quad (17)$$

therefore the variation of the orbital separation between the two components is negligible and is assumed to keep a constant value during the evolution of the binary system.

The evolution is followed from the onset of central H burning to the moment of Roche Lobe Overflow (RLOF). Starting from an initial solid body rotation, we then calculate the evolution of the angular velocity inside the model consistently accounting for the various transport mechanisms presented in Sect. 3 and for the tidal interactions between the two stars.

<sup>1</sup> <http://www-astro.ulb.ac.be/Netgen/>

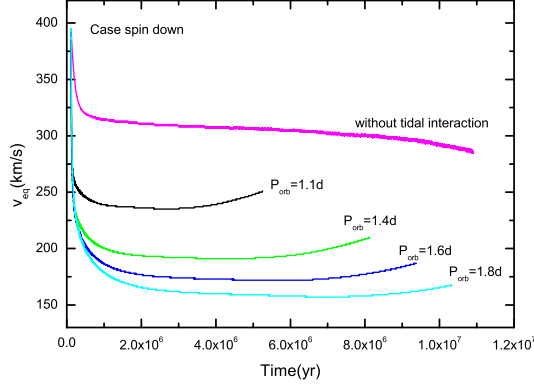


**Fig. 1.** Evolution as a function of time of the surface equatorial velocity for a  $15 M_{\odot}$  star with  $v_{\text{ini}}=0.6 v_{\text{crit}}$  and a  $10 M_{\odot}$  companion for different initial orbital periods. The case without any tidal interaction is also shown.

Unlike stellar winds, the tidal braking does not only spin down the star, but it may also spin it up. We have modeled the tidal mixing in two series of evolutionary sequences

- **Case spin down:** The orbital periods and the initial rotation velocities have been chosen so that tidal interaction spin down the primary. The initial velocity is chosen as  $v_{\text{ini}}/v_{\text{crit}}=0.6$ ,  $v_{\text{ini}}$  is the equatorial surface velocity on the ZAMS and  $v_{\text{crit}}$  is the critical velocity at the same stage (the critical velocity is defined as the equatorial velocity such that the centrifugal acceleration exactly balances the gravity at equator). The consequences of tidal braking were explored for different initial orbital periods ranging from 1.1 to 1.8 days. For comparison, a model starting with  $v_{\text{ini}}/v_{\text{crit}}=0.6$  on the ZAMS, with no account of tidal braking, has also been computed.
- **Case spin up:** The orbital periods and the initial rotation velocities have been chosen so that tidal interaction spin up the primary. The initial velocity is taken as  $v_{\text{ini}}/v_{\text{crit}}=0.2$ . The initial orbital periods were chosen between 0.9 and 1.4 days. A model without tidal interaction with  $v_{\text{ini}}/v_{\text{crit}}=0.2$  has also been computed.

## 5. Case spin down : tidal braking

### 5.1. Impact on rotation

The time evolution of the surface velocity is plotted for various orbital periods in Fig. 1. **We see the rapid decrease of the velocities due to tidal braking.** Synchronization is realised near the minimum of the curves. After that point, the angular velocity  $\Omega$  at the surface is maintained approximately at the value imposed by the orbital angular velocity and thus remains constant. Since, during the Main-Sequence phase, the radii of the star progressively increase, the surface velocities also slightly increase after synchronisation. From Fig. 1, we also see that:

- The surface velocity of tidally braked stars is much lower, at a given age, than the surface velocity of an isolated star starting its evolution on the ZAMS with the same initial velocity. This illustrates the well known fact that, for these orbital periods, the tidal interactions are very strong.

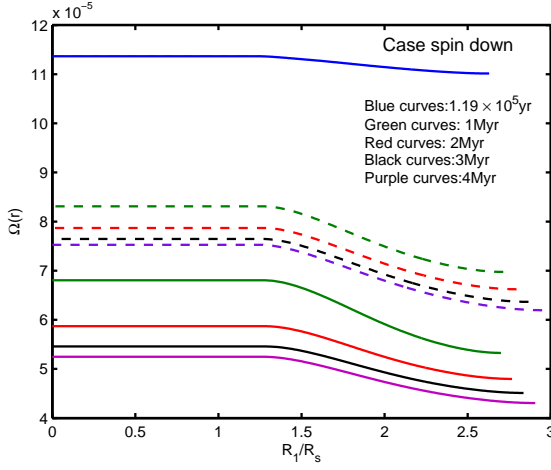


**Fig. 2.** Variation of the angular velocity as a function of the radius in solar units. The continuous lines refer to the spin down case with an orbital period equal to 1.8 days. The dashed curves correspond to the spin down case with an orbital period equal to 1.1 days. Different ages are plotted with different colors as indicated in the inset, for both the continuous and dashed lines. The curve corresponding to an age of 119 000 years is the same for the model in the system with an orbital period  $P$  of 1.1 days and in the one with an orbital period of 1.8 days.

- Synchronisation timescales are shorter in orbital systems with shorter periods, because tidal torques are stronger.
- At the time of synchronisation, lower surface velocities are evidently obtained in systems with longer orbital periods.

The evolution of the angular velocity inside models of different ages and in systems with various orbital periods is shown in Fig. 2 up to  $4 \cdot 10^6$  yr. We can see in the model with an orbital period,  $P_{orb} = 1.1$  days, how tidal braking imposes, after about 1 million years, an angular velocity at the surface converging around  $6.6 \times 10^{-5}$  s ( $\Omega = \frac{2\pi}{P} = 6.6 \times 10^{-5}$  s). The same kind of convergence occurs in the various models but at later times. **Clearly, the angular velocity is decreased everywhere in the interior of the star by tidal braking, not only at the surface (compare the continuous and dashed curves in Fig. 2 which show the differences due to different tidal torques; when the braking is stronger, the core is also more strongly slowed down). This comes from the coupling due mainly to meridional currents.** Most interestingly, some gradient of  $\Omega$  is maintained in the star at the time of synchronisation, as a result of meridional circulation as discussed below.

We may also compare the gradients of  $\Omega$  in the models with and without tidal interactions (see Figs. 3 and 4). First, we note from Fig. 4 that at the beginning of the braking, the gradients of  $\Omega$  are stronger in the tidally braked models. This will imply stronger mixing of the chemical elements before synchronisation. Second, we see that, after synchronisation (after about  $3.0 \cdot 10^6$  years), the gradients of  $\Omega$  are shallower in the tidal braked models.

This last situation results from the interplay of many physical processes. Indeed, there is an impressive number of effects influencing  $\Omega$  inside the models: the structural changes, the convective transport, the shear turbulence which tends to erode the  $\Omega$ -gradients, the meridional circulation which can smooth or build up the  $\Omega$ -gradients, the tidal effects which can remove or bring angular



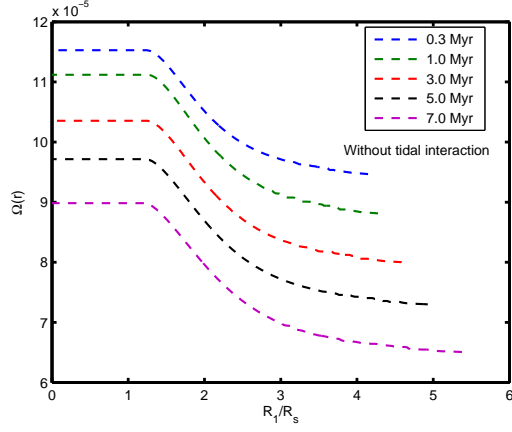


**Fig. 3.** Variation of the angular velocity ( $[\text{s}^{-1}]$ ) as a function of the radius and age inside a  $15 M_{\odot}$  model with  $v_{\text{ini}}/v_{\text{crit}} = 0.6$  computed without tidal interaction.

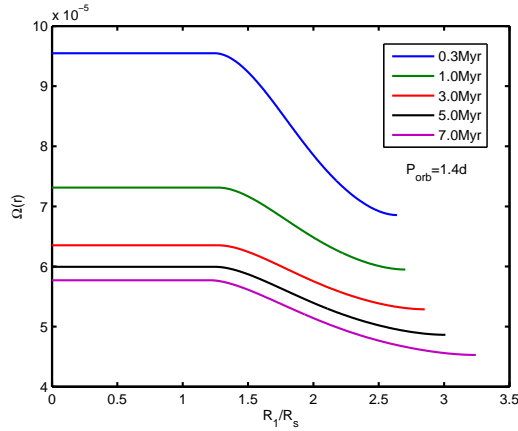


**Fig. 4.** Same as Fig. 3 for a  $15 M_{\odot}$  model with tidal braking. The companion is a  $10 M_{\odot}$  star and the orbital period is 1.4 days. Note that the maximum radius is not coinciding with the total radius of the star, only a portion of the interior is represented.

momentum. Mass loss can also remove angular momentum, especially when a magnetic field is present in outer layers. One of these effects may be dominant at a given moment at some point inside the star, while part of these effects or all can interact in other periods/regions of the star, so it is very difficult to identify a clear cut cause for the shallower  $\Omega$ -gradients in post synchronised systems.

Let us examine carefully the effects and behavior of the meridional circulation in relation with tidal effects. In Fig. 5, the variation as a function of the Lagrangian mass of  $U_2$ <sup>2</sup> is shown for the spin down Case with an initial orbital period of 1.4 days (look at the continuous lines). A negative value of  $U_2(r)$  corresponds to a net transport of angular momentum from the core to the envelope. A positive value corresponds to the reverse situation, i.e. to a net transport of angular momentum from the envelope to the core. We see that at the beginning of evolution (curves for the ages 1 and  $3 \cdot 10^6$  years in Fig. 5), the meridional circulation transports angular momentum from the core to the envelope. Thus, while tidal braking slows down the envelope, circulation tends to counteract

<sup>2</sup>  $U_2(r)$  is defined by  $U(r, \theta) = U_2(r)P_2(\cos \theta)$ , where  $U$  is the vertical component of the velocity of the meridional current,  $P_2$ , the second Legendre polynomial and  $\theta$ , the colatitude.

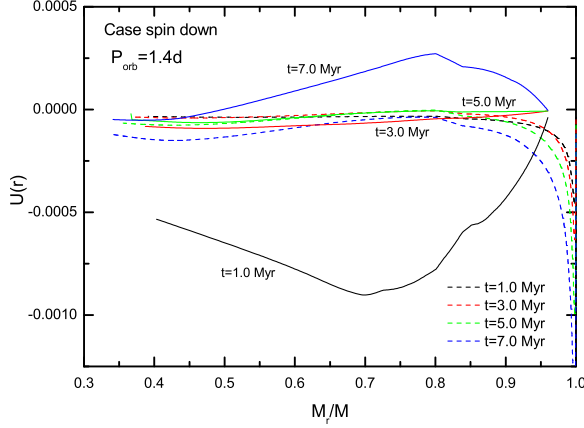


**Fig. 5.** Amplitude of the vertical component of the meridional circulation velocity in cm per second in a  $15 M_{\odot}$  model at various stages. The dashed lines correspond to a rotating model with  $\nu_{\text{ini}}=0.6 \nu_{\text{crit}}$  and computed with no account of tidal interaction. The continuous lines show the situation when tidal interactions are accounted for, assuming a close companion of  $10 M_{\odot}$  orbiting the primary with an initial period of 1.4 days. Different ages are plotted with different colors as indicated in the inset, for both the continuous and dashed lines. The different colors have the same significations as in Fig.2.

this effect by accelerating it. After about  $5 \cdot 10^6$  years, meridional circulation changes sign and the transport of angular momentum is from the envelope to the core, favoring the increase of the ratio between  $\Omega$  in the core and that in the envelope, at a time where synchronisation tends to homogenize the internal rotation

Comparing the variation of  $U_2$  in the models with and without tidal interaction, one sees important differences. In the model without tidal interaction, for the range of ages considered,  $U_2$  is always very negative, thus there is a net transport of angular momentum from the rapid spinning core to the slow rotating envelope. Such a process goes in the same direction as would do a diffusive process. In the model with tidal interactions, in a first period until  $\sim 5 \cdot 10^6$  years, meridional circulation transports angular momentum from the core to the envelope, as in the model without tidal interaction, but with much larger negative velocities, as can be seen in Fig. 5. Then, as the circulation changes sign, the transport of angular momentum goes from the envelope to the core. This last process can no longer be modeled through a diffusive process. Thus, it is essential to describe circulation currents as an advective process.

This redistribution of the angular momentum inside the star by meridional circulation has consequences for the synchronisation time. Since circulation tends to counteract the braking of the surface by the tidal torque, it increases the time needed for achieving synchronisation. **In Table 1, two times are indicated. In the second column  $t_{\text{rot}}$  is given for the various initial orbital periods and for ZAMS values. The third column shows the effective time at which  $\Omega=\omega_{\text{orb}}$  as given by the present evolutionary stellar models.**

**The values of  $t_{\text{rot}}$  are extremely short, much less than 1% of the Main-Sequence lifetime of a  $15 M_{\odot}$  star. This is quite consistent with the very small timescales obtained by de Mink et**

al. (2009) and also with the very rapid decrease of the surface velocity shown in our present models (see Fig. 1).

The effective time at which  $\Omega=\omega_{\text{orb}}$  is much longer than  $t_{\text{rot}}$  by large factors greater than 70. The main reason making this time longer is the outward transport of angular momentum by circulation, which counteracts tidal braking. It must be noted however that looking at Fig. 1, the decrease of the equatorial surface velocity is quite fast and from an observational point of view the star may be considered as synchronized well before the time at which one has the strict equality  $\Omega=\omega_{\text{orb}}$ . Thus, the present results do not contradict the observed fact that all binaries of the sample of B-type stars observed by Abt et al. (2002) with periods less than 2.4 days (18 stars) are synchronized.

The main consequences of these findings are :

- Tidal braking has a large impact on meridional currents, which in turn redistributes the angular momentum inside the star.
- $t_{\text{rot}}$  as defined above greatly underestimates the time needed for  $\Omega$  to become equal to  $\omega_{\text{orb}}$ .
- The gradient of  $\Omega$  is not flat when synchronisation is achieved.

**Table 1.** Synchronisation timescales,  $t_{\text{rot}}$ , as given by Eq. (6) for ZAMS values and time at which  $\Omega=\omega_{\text{orb}}$  from the numerical models for  $15 M_{\odot}$  starting with an initial equatorial velocity on the ZAMS equal to  $390 \text{ km s}^{-1}$ .

P	$t_{\text{rot}}$ (yr)	$t(\Omega = \omega)$ (yr)
1.1	27 400	1 900 000
1.4	38 000	3 440 000
1.6	54 900	4 580 000
1.8	77 800	5 400 000

## 5.2. Impact on the chemical composition and evolutionary tracks

Vertical shear turbulence is the main driver for chemical mixing. Let us see how the shear diffusion coefficient varies as a function of the Lagrangian mass coordinate in models with different tidal interactions (Fig. 6). At the beginning, the diffusion is quite small since the  $\Omega$ -gradients are very small. Then the braking produces a strong shear and the diffusion increases. One notes that after about 0.2 Myr, the shear diffusion coefficient is slightly larger in the model with the longer orbital period, indicating that stronger  $\Omega$ -gradients are produced by tidal interactions in these systems. This probably comes from the fact that torques in longer period systems are active over longer durations than in shorter period systems.

As a result of the  $\Omega$ -gradients induced by the tidal interactions, the surface becomes enriched in nitrogen (see Fig. 7). In stars with tidal braking a given enrichment is reached for larger values of the surface gravity than in single star starting with the same initial rotation, indicating a much more efficient mixing. Interestingly enough, these models produce relatively high nitrogen abundances for high  $\log g$  values, but low surface velocities (see Fig. 1). Thus, tidal mixing strongly changes

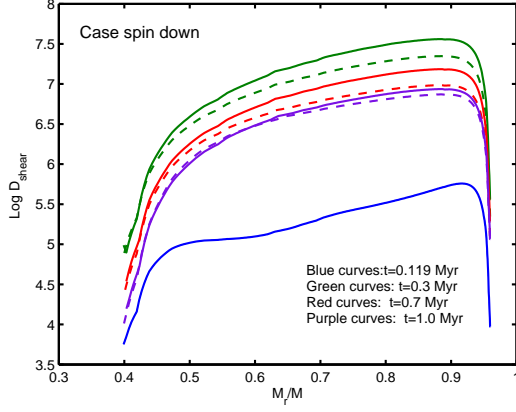


**Fig. 6.** Variation as a function of the Lagrangian mass coordinate of the shear diffusion coefficient in the radiative envelope of our  $15 M_{\odot}$  model. The continuous lines refer to the spin down case with an initial orbital period of 1.8 days. The dashed lines show the case when the initial orbital period is equal to 1.1 days. The curves for the periods equal to 1.1 and 1.8 days, corresponding to an age of 119 000 years, are the same and thus are superposed. The different colors has the same significations as in Fig. 2.

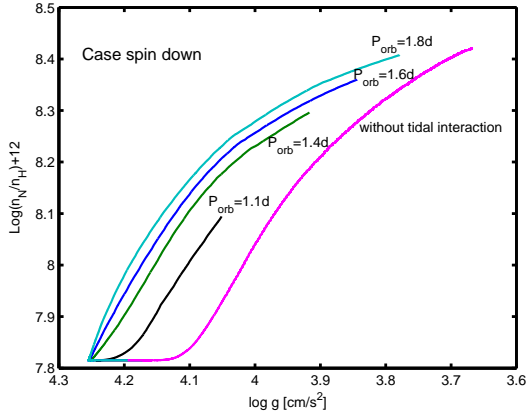


**Fig. 7.** Variation as a function of time of the ratio in number, at the surface, of nitrogen to hydrogen for  $15 M_{\odot}$  stellar models with (spin down case) and without tidal interactions. The curves are labeled with the values of the initial orbital period.

the correlation between surface velocity, nitrogen abundance and surface gravity with respect to the correlations obtained in models without tidal mixing.

In Fig. 8, the analog of Fig. 7 is shown but for the surface enrichments in helium. One sees the same qualitative behaviors as for nitrogen, but with smaller amplitudes, likely not observable.

The different mixings undergone by the stars produce internal compositions which greatly differ at a given age. This can be seen in Fig. 9 where the variations of the mass fraction of hydrogen in our  $15 M_{\odot}$  are shown at a given age for various efficiencies of the tidal braking. We see that in short period systems, the hydrogen profiles is less affected than in longer period systems. This directly results from the point raised above indicating that shear mixing is more efficient in longer period systems.

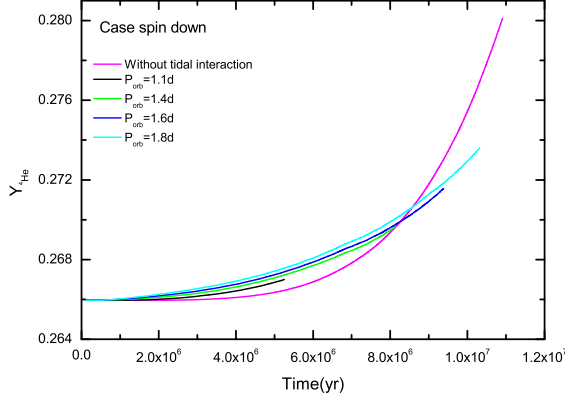


**Fig. 8.** Variation as a function of time of the surface helium mass fraction for  $15 M_{\odot}$  with (spin down case) and without tidal interactions. The curves are labeled with the values of the initial orbital period.

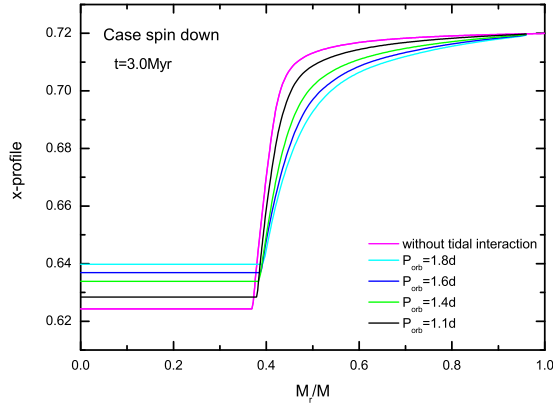


**Fig. 9.** Variation as a function of the Lagrangian mass coordinate of the mass fraction of hydrogen in  $15 M_{\odot}$  models with (spin down case) and without tidal interaction at the same age during the Main-Sequence phase. Curves for different initial orbital periods are shown.

The consequences of these various hydrogen compositions on the evolutionary tracks in the HR diagram can be seen in Fig. 10. **All tracks with tidal interactions are shifted to the blue with respect to the track without tidal interaction. The longer the initial period, the greater the blueshift is, consistent with larger mixing in longer period systems.** The mass-age-luminosity relation is significantly influenced by tidal mixing, in the sense of an overluminosity for a given mass in the case of tidal braking.

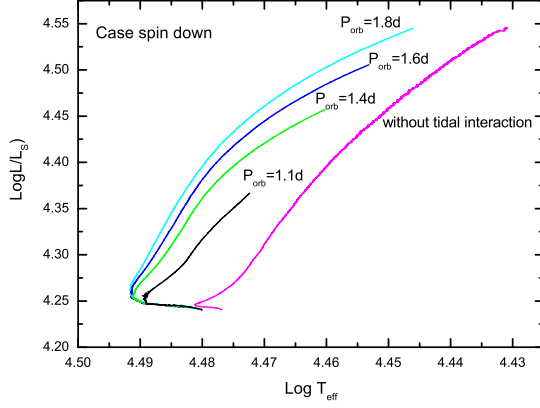


**Fig. 10.** Evolutionary tracks for  $15 M_{\odot}$  models with (spin down case) and without tidal interaction. Curves for different initial orbital periods are shown. For close binaries, only the part of the track corresponding to the period before the Roche Lobe Overflow is plotted.

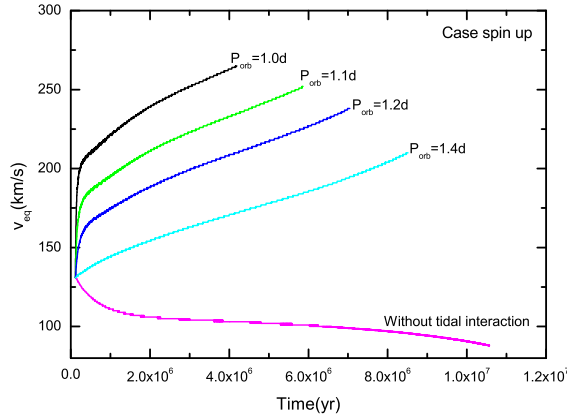


**Fig. 11.** Evolution as a function of time of the surface equatorial velocity for a  $15 M_{\odot}$  star with  $v_{\text{ini}}=0.2 v_{\text{crit}}$  and a  $10 M_{\odot}$  companion for different initial orbital periods. The case without any tidal interaction is also shown.

## 6. Case spin up : tidal acceleration

### 6.1. Impact on rotation

Now we discuss situations when the primary is spun up by tidal interactions. Figure 11 shows how the surface velocity varies as a function of time in case of tidal spin up. The models with tidal interactions rapidly become fast rotators under the influence of their companions. As expected, when the orbital period is short, the surface velocity increase very rapidly and reaches a high value.

The evolution of  $\Omega$  inside different tidally spin up models are shown in Fig. 12. **We can see how tidal interaction imposes the surface angular velocity to approach the value of the orbital velocity which is  $7.26 \cdot 10^{-6} \text{ s}^{-1}$  for the system with an orbital period of 1.0 days, and  $5.19 \cdot 10^{-6} \text{ s}^{-1}$ , for the system with an orbital period of 1.4 days. Actually, one sees that these systems**

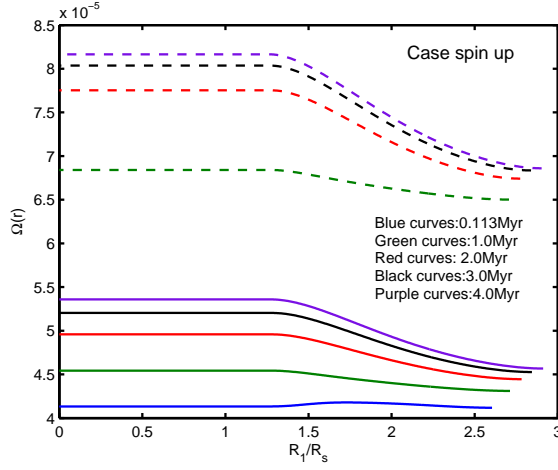


**Fig. 12.** Variation of the angular velocity as a function of the radius in solar units. The continuous lines refer the spin up case with an orbital period equal to 1.4 days. The dashed curves correspond to the spin up case with an orbital period equal to 1.0 days. Different ages are plotted with different colors as indicated in the inset, for both the continuous and dashed lines. The curves for the periods equal to 1.0 and 1.4 days, corresponding to an age of 113 000 years, are the same and thus are superposed.

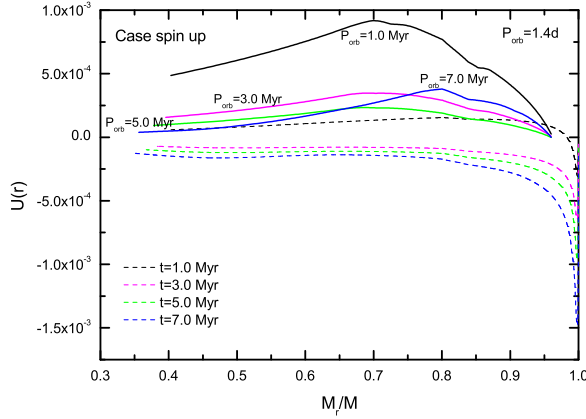


**Fig. 13.** Same as Fig. 1 for a  $15 M_{\odot}$  model with  $v_{\text{ini}}=0.2 v_{\text{crit}}$ . The continuous lines show the situation when tidal interactions are accounted for assuming a close companion of  $10 M_{\odot}$  orbiting the primary with an initial period of 1.4 days. The dashed lines correspond to a rotating model computed with no account of tidal interaction. The different colors have the same significations as in Fig.2.

**reach Roche Lobe Overflow before being synchronized.** We see that the gradient of  $\Omega$  increases slightly when time goes on.

In Fig. 13, the radial component of the vertical velocity of meridional circulation is shown. During the whole period considered, circulation transports angular momentum from the envelope to the core. Thus, we obtain in case of tidal spin up, the same kind of general behavior we obtained in case of tidal spin down: meridional circulation counteracts the effect of the tidal interaction. When

the surface is spun down, circulation tends to accelerate it, and when the surface is spun up, it tends to slow it down. Thus, for both tidal spin up and down, the synchronisation times are increased due to the redistribution of the angular momentum inside the star by meridional circulation.

**From Table 2, we see that the synchronization timescales,  $t_{\text{rot}}$ , is much shorter than the time at which the Roche Lobe Overflow (RLOF) occurs. On the other hand, the RLOF occurs before the effective time when  $\Omega = \omega_{\text{orb}}$ . That means that the values shown in the third column of Table 2 are lower limit for the times  $t(\Omega = \omega_{\text{orb}})$ . Thus we have a very similar situation than in the case of spin down, where  $t_{\text{rot}}$  is much smaller than the time at which  $\Omega = \omega_{\text{orb}}$ . In contrast however with the case of spin down, here we cannot say that very rapidly  $\Omega$  converges towards values near  $\omega_{\text{orb}}$ . It does therefore appear more difficult to reach synchronization in tidally spin up systems. The reason is likely the following ones: An inwards transport of a given mass carries more angular momentum than an outwards transport of the same mass, because the specific angular momentum increases as a function of the distance to the center. Thus, it is easier for the circulation to slow down the surface when it is accelerated by the tidal interaction than for the opposite situation in the case of spin down.**

**Table 2. Synchronisation timescales,  $t_{\text{rot}}$ , as given by Eq. (6) for ZAMS values and time at which a Roche Lobe Overflow occurs for  $15 M_{\odot}$  starting with an initial equatorial velocity on the ZAMS equal to  $130 \text{ km s}^{-1}$ .**

P	$t_{\text{rot}}$ (yr)	$t(\text{RLOF})$ (yr)
1.0	26 400	4 167 000
1.1	57 200	5 856 000
1.2	122 700	7 029 000
1.4	608 400	8 496 000

In this case of tidal spin-up, we also see that a proper advective treatment of meridional circulation is needed for the whole period. A diffusive treatment would not account for the direction of the transport of angular momentum at any moment and thus would even produce effects with the wrong sign. Incidentally, Fig. 13 also shows that the velocity of the circulation currents tend to decrease with time. This reflects the fact that the gradient of  $\Omega$  increases slightly when time goes on (see Fig. 12).

## 6.2. Impact on chemical composition

Tidal acceleration boosts the shear diffusion and the surface nitrogen enrichments as can be seen in Figs. 14 and 15. From Fig. 14, one sees that the shear diffusion coefficient is larger in shorter period systems. This is the reverse of what is obtained in systems which are tidally spun down. In “spin down” system, we had larger  $D_{\text{shear}}$  in longer period systems as a result of a smaller, but longer active torque acting on the surface. In “spin up” systems, we have larger  $D_{\text{shear}}$  in shorter period systems as a result of a shorter active, but stronger torque acting on the surface.

As a consequence of the shears in tidally interacting systems, strong surface enrichments in nitrogen are resulting, as can be seen in Fig. 15. A given nitrogen enhancement is obtained earlier,



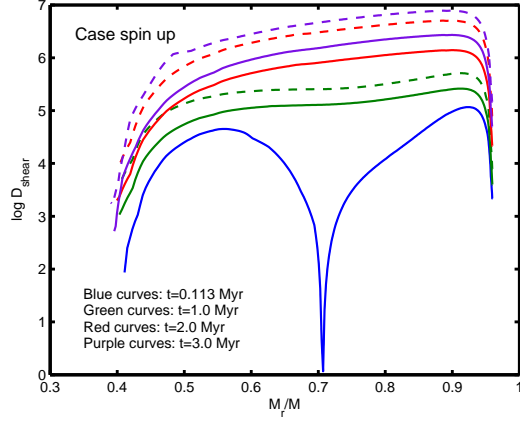


**Fig. 14.** Variation as a function of the Lagrangian mass coordinate of the shear diffusion coefficient in the radiative envelope of our  $15 M_{\odot}$  model. The continuous lines refer to the spin up case with an initial orbital period of 1.4 days. The dashed lines show the case when the initial orbital period is equal to 1.0 days. The curves for the periods equal to 1.0 and 1.4 days, corresponding to an age of 113 000 years, are the same and thus are superposed. The different colors have the same significations as in Fig.2.

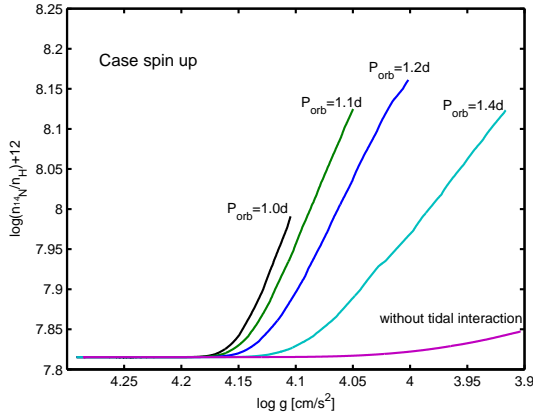


**Fig. 15.** Variation as a function of time of the ratio, in number, of nitrogen to hydrogen at the surface of a  $15 M_{\odot}$  stellar model with (spin up case) and without tidal interactions. The curves are labeled with the values of the initial orbital period.

i.e. for lower surface gravity values in shorter period systems. The surface helium enrichments reflect the same trend, but with limited amplitudes (see Fig. 16). The variations of the mass fraction of hydrogen are shown in Fig. 17. Consistently with other results, we see that for smaller initial periods, the effects of the tidal spinning up are stronger, again due the higher  $\Omega$ -gradients.

The impact on the evolutionary tracks can be seen in Fig. 18. There is a shift of tidally accelerated models towards redder positions compared to the model without tidal interaction, for periods shorter than about 1.2-1.3 days. It comes from the fact that globally the stars is rapidly spun up and the centrifugal acceleration becomes non negligible. The centrifugal acceleration balances the gravity. This tends to make the star to follow an evolution corresponding to a lower initial mass, thus with a lower luminosity and being redder. For the period 1.4 days, one sees that the track is

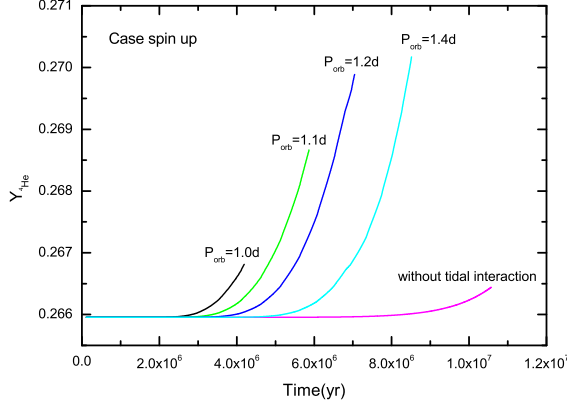


**Fig. 16.** Variation as a function of time of the surface helium mass fraction for  $15 M_{\odot}$  with (spin up case) and without tidal interactions. The curves are labeled with the values of the initial orbital period.

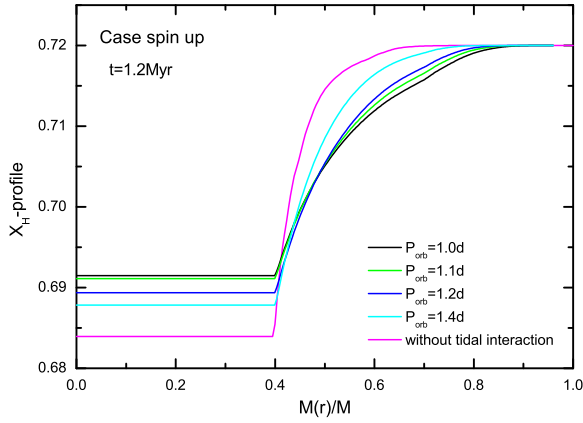


**Fig. 17.** Variation as a function of the lagrangian mass coordinate of the mass fraction of hydrogen in  $15 M_{\odot}$  models with (spin up case) and without tidal interaction at the same age during the Main-Sequence phase. Curves for different initial orbital periods are shown.

only very slightly overluminous with respect to the track without tidal interaction. In that case, the hydrostatic effects and those of chemical mixing are more or less compensating each other. This produces a track not far from the one computed without tidal interaction.

## 7. Conclusions and observable consequences

From the above results, we can deduce some interesting general trends and consequences :

- 1) At least up to the RLOF, the direction of the meridional circulation is always in a sense that counteracts the effects of the tidal interaction. Meridional currents are spinning up the surface when it is braked down (spin down case), and are braking it down when it is accelerated (spin up case).

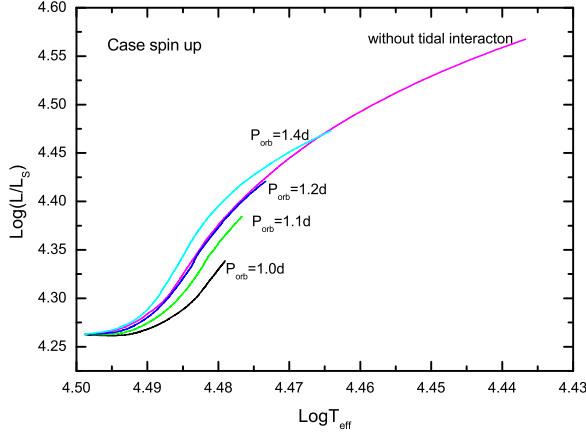


**Fig. 18.** Evolutionary tracks for  $15 M_{\odot}$  models with (spin up case) and without tidal interaction. Curves for different initial orbital periods are shown. For close binaries, only the part of the track corresponding to the period before the Roche Lobe Overflow is plotted.

This illustrates how circulation is driven by what happens at the surface, tending to restore previous equilibrium. These trends seem to be a general property of meridional circulation.

2) For correctly modeling the effects of tidal interactions, a proper account of the transport of angular momentum by advection through meridional currents is essential.

3) **The effective time for obtaining  $\Omega = \omega_{\text{orb}}$  may extend over periods covering a significant fraction of the Main-Sequence lifetime.**

4) Whatever tides brake down the surface or spin it up, they boost the shear diffusion coefficient and the surface nitrogen enrichments.

5) How these effects vary as a function of the initial period depends on whether tidal interactions brake down or spin up the star. In case of braking down, the effects obtained at the end of synchronisation on the surface enrichments are enlarged when the initial period increases. The contrary occurs in case of tidal spin up.

From the point of view of possible interesting observable consequences of tidal interactions, we can note :

1) **Spin-up systems studied here encounters RLOF before being synchronized.**

2) The possibility through asteroseismology to probe the internal rotation rate of stars during their synchronization period or after synchronization (but before any RLOF) would provide extremely interesting constraints on the present models.

3) Tidal braking produces stars which are strongly nitrogen rich, slowly rotating and presenting a high surface gravity. Such a braking can be invoked to explain some slow, non evolved rotators with strong nitrogen enrichment.

4) Tidal spinning up may produce fast rotators before the RLOF episode. After RLOF, the loss of the envelope will probably considerably slow down the star. Thus it will be likely not possible to produce fast rotators following a homogeneous evolution through tidal interaction. The process can be initiated by tidal spin up but, at a given point, RLOF will stop it.

5) In tidal spin up, part of the angular momentum acquired by the primary will be locked into the core due to the redistribution of the angular momentum. Is there any link with Gamma Ray Bursts? This has to be further studied in forthcoming works.

Let us note that the results would be very different in case some process would force the star to rotate as a solid body in its interior (this might be due for instance to a strong internal magnetic field). We can suspect that the results would be qualitatively similar to those obtained when a magnetic braking is applied at the surface of a solid body rotating star (Meynet et al. 2011): a very fast change of the surface velocity (short time for obtaining  $\Omega = \omega$ ) and no tidal mixing during the synchronisation period. This will be studied in a forthcoming paper.

*Acknowledgements.* This work was sponsored by Key Laboratory for the Structure and Evolution of Celestial Objects, Chinese Academy of Sciences, (Grant No. OP201107), the Key Foundation at Guizhou education department (No 2010002). We thank Dr. Patrick Eggenberger for having made available his routine for the change of angular momentum in the outer layers and for very useful remarks helping to improve this paper. **We are very grateful to professor Jean-Paul Zahn (referee) for his valuable suggestions and insightful remarks, which have improved this paper greatly. Also we thank the editor for his/her professional and excellent work.**

## References

- Abt, Helmut A., Levato, Hugo, Grosso, Monica, 2002, ApJ, 573, 359A
- Angulo, C., Arnould, M., Rayet, M., et al. 1999, Nucl. Phys. A, 656, 3 Angulo, C. & Descouvemont, P. 2001, Nucl. Phys. A, 690, 755
- Asplund, M., Grevesse, N., & Sauval, A. J. 2005, in ASPC, Vol. 336, Cosmic Abundances as Records of Stellar Evolution and Nucleosynthesis, ed. T. G. Barnes, III & F. N. Bash (San Francisco: ASP), 25
- Chaboyer, B. & Zahn, J.-P. 1992, A&A, 253, 173
- Cunha, K., Hubeny, I., & Lanz, T. 2006, ApJ, 647, L143 de Jager, C., Nieuwenhuijzen, H., & van der Hucht, K. A. 1988, A&AS, 72, 259
- Denissenkov P.A., Ivanova N.S., Weiss A., 1999, A&A 341, 181
- de Mink, S. E., Cantiello, M., Langer, N., Pols, O. R., Brott, I., Yoon, S.-Ch., 2009, A&A, 497, 243D
- de Mink et al. 2013, ApJ, 764, 166
- Endal, A. S. & Sofia, S., 1976, ApJ, 210, 184
- Ekström, S., Georgy, C., Eggenberger, P., Meynet, G., Mowlavi, N., Wyttenbach, A., Granada, A., Decressin, T., Hirschi, R., Frischknecht, U., and 2 coauthors, 2012, A&A, 537A, 146E
- Heap, S. R., Lanz, T., Hubeny, I., 2006, ApJ, 638, 409H
- Heger, A., Langer, N. and Woosley, S.E., 2000a, ApJ, 528, 368
- Heger, A., Langer, N., 2000b, ApJ, 544, 1016
- Huang R. Q., 2004a, A&A, 422, 981
- Huang R. Q., 2004b, A&A, 425, 591
- Hunter, I., Brott, I., Langer, N., Lennon, D. J., Dufton, P. L., Howarth, I. D., Ryans, R. S. I., Trundle, C., Evans, C. J., de Koter, A., Smartt, S. J., 2009, A&A, 496, 841H
- Kippenhahn, R., Thomas, H.-C., Stellar Rotation, Proceedings of IAU Colloq. 4, held at the Ohio State University, Columbus, Ohio, 8-11 September, 1969. Edited by Arne Slettebak. Gordon and Breach Science Publishers, 1970., p.20
- Langer N., 1998, A&A, 329, 551
- Langer, N. & Maeder, A. 1995, A&A, 295, 685,
- Maeder, A. 1997, A&A, 321, 134
- Maeder, A. 1999, A&A, 347, 185
- Maeder, A. 2009, Physics, Formation and Evolution of Rotating Stars (Berlin Heidelberg: Springer Verlag)
- Maeder, A. & Meynet, G. 2000, ARA&A, 38, 143M
- Maeder, A. & Meynet, G. 2001, A&A, 373, 555
- Maeder, A., 2003, A&A, 399, 263M

- Maeder, A. & Meynet, G. 2005, A&A, 440, 1041
- Maeder, A. & Meynet, G. 2012, Reviews of Modern Physics, 84, 25
- Maeder, A. & Zahn, J.-P. 1998, A&A, 334, 1000
- Mathis, S., Palacios, A., Zahn, J.-P., 2004, A&A, 425, 243M
- Mathis, S., Zahn, J.-P., 2004, A&A, 425, 229M
- Mahy et al. 2009, A&A, 502, 937
- Meynet, G. & Maeder, A. 1997, A&A, 321, 465
- Meynet, G. & Maeder, A. 2000, A&A, 361, 101
- Meynet, G., Eggenberger, P. & Maeder, A., 2011, A&A, 525L, 11M
- Schaller, G., Schaerer, D., Meynet, G., & Maeder, A. 1992, A&AS, 96, 269
- Przybilla, N., Farnsteiner, M., Nieva, M. F., Meynet, G., Maeder, A., 2010, A&A, 517A, 38P
- Song, H.F., Zhong, Z. & Lu, Y. 2009, A&A, 504, 161
- Song, H.F., Lu, Y. & Wang, J. Z., 2011, PASJ, 63, 835
- Sana et al. 2013, A&A 550, 107
- Talon, S. & Zahn, J.-P. 1997, A&A, 317, 749
- Toledano, O., Moreno, E., Koenigsberger, G., Detmers, R., Langer, N., 2007, A&A, 461, 1057T
- Walborn, N. R., 1976, IAUS, 72, 153W
- Yoon, S.-C., Woosley, S. E. & Langer, N., 2010, ApJ, 725, 940Y
- Zahn, J.-P. 1966, AnAp, 29, 489
- Zahn, J.-P. 1975, A&A, 41, 329
- Zahn, J.-P. 1977, A&A, 57, 383
- Zahn, J.-P. 1992, A&A, 265, 115